Journal of Global Positioning Systems (*2023*)
Vol. 19, Joint No. 1 & No. 2: 36-55
DOI: 10.5081/jgps.19.1.36

Practical Studies of Accuracy Enhancement Techniques for Terrestrial Mobile LiDAR Point Clouds in Engineering Surveys

Wang, Jianguo[1]; Guannan Liu✉[1,2]; Baoxin Hu[1]
jgwang@yorku.ca; qqliuguannan@gmail.com; baoxin@yorku.ca
[1] Department of Earth and Space Science and Engineering, York University, Canada
[2] Ministry of Transportation of Ontario, Canada
✉ Corresponding author

Abstract: Improving the accuracy of Terrestrial Mobile LiDAR (TML) data has been a challenge in Engineering Surveys. This research aims at how to innovatively enhance the accuracy of TML solutions through post-processing toward meeting high accuracy specifications in Engineering Surveys. Three techniques are described and implemented. Firstly, the linear feature-enhanced 3D Conformal Coordinate Transformation (3DCCT) is developed by employing ground control points (GCPs) together with linear feature constraints. Secondly, a two-stage Multistrip Adjustment (MA) technique is proposed that first co-register the overlapped TML strips using tie points and tie features extracted from them and then adjust the co-registered LiDAR data by applying the feature enhanced 3DCCT. Lastly, a post-processing technique for calibrating the LiDAR boresight errors of a terrestrial LiDAR system is tested out by using its own point clouds. Their usage has been strategically studied through their applications to field-test data. Specifically, multiple scenarios have been tested, analysed, and compared in terms of the usage of GCPs, the effect of feature constraints, MA and the effect of boresight error compensation etc. As shown from the results, their utilization is encouragingly contributing to the accuracy improvement of TML data towards the high accuracy demand for Engineering Surveys. A practical implementation dataflow is outlined at the end of this manuscript.

Key Words: terrestrial mobile LiDAR, engineering surveys, accuracy enhancement, 3D conformal transformation, ground control point, linear features, multistrip adjustment, post-processed boresight calibration.

1. Introduction

A Terrestrial Mobile LiDAR (TML) system is a high-tech industrial product and mostly has one or more laser scanners directly georeferenced by a multisensor (GNSS/IMU/Odometer//Cameras) integrated kinematic positioning and navigation system mounted on a moving vehicle. Since it was introduced to Engineering in the early 2000s [Glennie, 2009; Guan, et al., 2016], a great variety of application-oriented case studies have progressively been advancing this technique in terms of its practicability, efficiency, and performance [Slob & Hack, 2004; Durrieu et al., 2008; Gräfe, 2008; Hofmann & Brenner, 2009; Jaakkola et al., 2010; Sherif et al., 2011; Esfandabadi, 2018; Di Stefanoa et al., 2021; Kurdi et al., 2023; Elsayed & Shaker, 2023]. The technique comes with high potential over other traditional surveying techniques, such as total station and aerial photogrammetry for generating high-resolution 3D models from traditional digital surface/elevation models to 3D models for geospatial mapping database, urban planning, transportation corridor surveys, engineering design, rail surveys, utility mapping and structure inspection, monitoring, to management etc. in complex engineering projects [Glennie, 2009; Esfandabadi, 2018; Kurdi et al., 2023; Elsayed & Shaker, 2023]. Encouragingly, such data are a totally immersive 3D view of the objects and surroundings [Rybka, 2011; Guan et al., 2016]. In practice, this technique has gradually been accepted by professional surveyors as an automatic and efficient novel surveying technique that can decrease the on-site safety risk and increase productivity compared with traditional surveying instruments.

Under favourable conditions, the absolute 3D positioning accuracy of a point cloud produced by a TML system could be as good as ±2cm, e.g., ±2cm (georeferencing) and 5mm (range) for StreetMapper V (www.igi-systems.com), ±2cm (good GPS with PDOP <3) for LYNX HS600 (teledyneoptech.com), and ±2.0cm (microscale 3D data) for FGI ROAMER (laserscanning.fi) etc. per manufacturers. Although the range accuracy of a LiDAR sensor can be as high as a few mm for a distance up to 100m, the absolute accuracy of a scanned point mostly lies on the

accuracy of the direct georeferencing system, a GNSS and IMU based multisensor integrated kinematic positioning system, as well as the remaining systematic errors such as the errors in lever arms and boresight angles. Apparently, the accuracy level of the data acquired by a TML system could be confined to the aforementioned error sources. There have been plenty of intensive accuracy analyses of TML techniques conducted from various aspects and via different TML products [Glennie et al., 2006; Glennie, 2007; Kadatskiy, 2011; Hu et al., 2012; Hu et al., 2013; Leslar et al., 2014; Liu, 2015; Leslar, 2016; Kenza & Mohmamed, 2018; Khanal et al., 2020]. In terms of accuracy satisfaction, it is a challenging task to apply a TML system to specific engineering surveying applications, e.g., transportation etc. According to MTO [2016], engineering surveys are generally a necessity at the detail design stage where accuracies are at the 1 to 2-cm-level on hard surfaces, and 5 to 10-cm-level on soft surfaces with respect to the nearest project control. Specifically, the accuracy requirement (95% confidence level) with the roadway features, from Asphalt Edges, Bridge deck, Crown of road, Curbs, Driving Lane – Edge, Gutter Edge, to Pavement Edge, can be as high as ±2cm horizontally and vertically regardless of the field survey method used [MTO, 2016]. On the one hand, the required data accuracy for the above-mentioned specific applications in Engineering surveys is overall higher than an LML system can deliver under average field working conditions. On the other hand, there exists a good opportunity to enhance the raw data accuracy through post processing either by taking advantage of multistrip merging process, the extracted features or even by introducing a limited number of GCPs wherever necessary, especially in terms of compensating for remaining systematic errors. Up to now, how to efficiently further enhance the accuracy of the acquired TML data through post-processing is an active research topic. Resultingly, the objective of this manuscript is focused on how to improve the accuracy of raw LML data significantly and efficiently through post processing. Frankly, the goal of this research is not so much about how to improve the accuracy of LML data to meet a specific accuracy requirement than about how to significantly improve the accuracy of an LML point cloud in practice.

Right after this introduction, Section 2 proposes and describes three techniques: 1) Linear Feature-Enhanced 3D Coordinate Conformal Transformation (3DCCT); 2) Multistrip Adjustment (MA); and 3) Post-processed LiDAR boresight calibration. Their implementation is detailed in Section 3. In Section 4, test data are first overviewed and then the results from three specific analyses: GCP Usage Optimization, Multistrip Adjustment inclusive of LFE3DCCT and accuracy improvement with the aid of point cloud based post-processed LiDAR boresight calibration (PPLBC). At the end, Section 4 concludes the manuscript.

2. Methodology

The key to the accuracy enhancement of LML point clouds is how to reduce the comprehensive influence of all the remaining systematic errors in the georeferencing process, sensor calibration of lever arms, boresight angles and so on in general. The proposed three techniques are presented here below.

2.1 Linear Features-Enhanced 3D Conformal Coordinate Transformation

The initial thought would be to take advantage of the mathematic relationships of the common points through their dual coordinates surveyed as ground control points (GCPs) and delivered by a mobile LiDAR system because it preserves the orientation and shape of objects that can result in parameters to compensate for the remaining systematic errors in a TML solution. Using ground control points (GCPs) is an effective way to remove some of the leftover systematic errors, improve the absolute accuracies of TML solutions, or make up for poor GPS performance, even GPS outages. The positioning accuracy of the LiDAR solution could significantly be improved to a specific level. However, the associated cost with setting up GCPs is relatively high, so the benefit of the mobile LiDAR technique as a cost-effective solution could significantly be compromised. Accordingly, the spatial locations of the existing characteristic (natural and/or artificial) points, lines and planes, such as the corners of buildings, windows, traffic lights, signs and posts, pavement markings, flat surfaces/walls, building facades and stop bars etc., could be employed to reduce even eliminate the cost and/or access authorization request for setting up targets in the field, i.e. to enhance the performance resulted by limited expensive GCPs. A linear features-enhanced 3DCCT was developed in the form of a general combined Least-Squares adjustment (i.e., 3DCCT with GCPs as conditional adjustment with parameters and linear features as additional constraints).

In general, the functional model for 3DCCT with an arbitrary common point *i* presented by $(X_i, Y_i, Z_i)^1$ in frame 1 and $(X_i, Y_i, Z_i)^2$ in frame 2 is given as follows:

$$\begin{pmatrix} X_i \\ Y_i \\ Z_i \end{pmatrix}^2 = \begin{pmatrix} X_T \\ Y_T \\ Z_T \end{pmatrix}_1^2 + sR(\theta_1, \theta_2, \theta_3) \begin{pmatrix} X_i \\ Y_i \\ Z_i \end{pmatrix}^1 \quad (1)$$

wherein (X_T, Y_T, Z_T), s and $(\theta_1, \theta_2, \theta_3)$ are the three translations, one scale, and three rotation angles from frame 1 to frame 2 while $R(\theta_1, \theta_2, \theta_3)$ is the rotation matrix of $(\theta_1, \theta_2, \theta_3)$ and $(X_i, Y_i, Z_i)^1$ and $(X_i, Y_i, Z_i)^2$ are six coordinate measurements.

The usage of line and plane features is illustrated in Fig. 1. To utilize the linear features, they are added to (1) as constraints. For an arbitrary point (X_j, Y_j, Z_j) on a given line (Fig. 1(a)), one has its functional form as

$$\frac{X_j - X_{l0}}{b_1} = \frac{Y_j - Y_{l0}}{b_2} = \frac{X_j - Z_{l0}}{b_3} \quad (2)$$

wherein $(b_1, b_2, b_3)^T$ is the unit vector parallel with the line subject to $b_1^2 + b_2^2 + b_3^2 = 1$, $(X_{l0}, Y_{l0}, Z_{l0})^T$ is the centroid of the being applied points (two or more points for applying the Least-Squares Principle) on the line. Similarly, for an arbitrary point (X_j, Y_j, Z_j) on a given plane (Fig. 1(b), one has its normal form as

$$a_1(X_j - X_{p0}) + a_2(Y_j - Y_{p0}) + a_3(Z_j - Z_{p0}) = 0 \quad (3)$$

wherein $(a_1, a_2, a_3)^T$ is the unit vector perpendicular to the plane with $a_1^2 + a_2^2 + a_3^2 = 1$, $(X_{p0}, Y_{p0}, Z_{p0})^T$ is the centroid of the being applied points (three or more points for applying the Least-Squares Principle) on the plane.

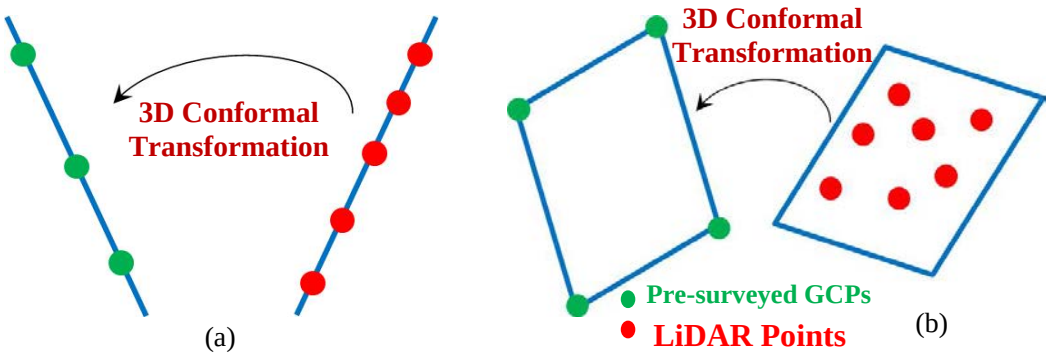

Fig. 1: Utilization of line and plane feature constraints in 3DCCT
(a) a straight line feature. (b) a planar patch feature.

For more details about the 3DCCT formulation and the Conditional Least-Squares Method with Constraints and Parametric Least-Squares Method with Constraints, refer to [Wang, et al., 2019; Liu, 2013].

In a practical way, we have considered how to implement the linear features-enhanced 3DCCT. First, the error effects on the coordinates of individual LiDAR points are apparently non-uniform because of the orientation and boresight angles based on the error analysis [Leslar, 2016; Leslar, et al., 2016; Leslar, et al., 2014; Hu et al., 2013]. Thus, the 3D conformal transformation may not be valid for a large stretch of data. For instance, the errors in the 3D mobile LiDAR point clouds may not be uniform horizontally and vertically. Moreover, the usage of the limited expensive GCPs needs to be optimized in terms of density and ideal distribution to employ those measurements efficiently and effectively. On one hand, it is desirable to choose natural targets placed not too far from each other and well distributed spatially to ensure that the transformation based on the targets indeed improves the LiDAR data accuracy. On the other hand, the required number of GCPs could be reduced, or the shortage even the absence of GCPs may be compensated for in some areas with the aid of feature constraints to achieve the minimal required accuracy.

2.2 Multistrip Adjustment

The multiple strips of data points for each scan area are often collected with airborne LiDAR missions in order to avoid gaps and reach the required point density. Since the objects surveyed can be large and complex-shaped, a series of scans from various directions is necessary to capture the complete representation of object geometry [Reshetyuk 2006]. Obviously, the adjacent LiDAR strips usually show discrepancies in overlapping areas due to the systematic errors in the LiDAR point cloud. Such discrepancies are caused by missing or improperly performing the system calibration and operation. Thus, it usually produces problems in extracting meaningful information and affects the quality of the final product [Lee et al., 2007]. Several strip adjustment methods were proposed for evaluating and improving the quality of airborne LiDAR data [Kilian et al., 1996; Crombaghs et al., 2000; Vosselman, 2002; Filin 2003; Kornus et al., 2003; Bretar et al., 2004; Kager, 2004; Pfeifer et al., 2005; Kersting et al., 2008; etc.]. The difficulty of implementing strip adjustment lies primarily in the irregular spatially distributed points. In each strip, the same object space is randomly sampled in the spatial domain [Shan and Toth, 2008]. The linear features have been chosen as conjugate features because they could be accurately extracted from man-made structures in urban areas and more easily than the

point features. Yousif et al. [2010] illustrated how to apply the data assimilation theory to enhance the 3D georeferencing accuracy as well as fine-tune the radiometric intensity by means of exploiting the correlation between two oppositely collected datasets over the same study area, which could combine two different datasets or models of the same phenomenon to achieve the best estimate of the true state. Thus, the performance of a TML system performance could also be improved by taking advantage of two or more data strips with sufficient overlapping collected from different runs.

In this research, multistrip adjustment (MA) was utilized as an additional tool to refine the directly-georeferenced TML point clouds by taking advantage of the overlapped data strips and the repeatedly acquired datasets in the same working area with the help of tie points and tie features [Liu, 2015]. Its main objective is to align the adjacent strips using both tie points and tie features by minimizing the impact of some of the systematic errors in the LiDAR system parameters towards improving the compatibility among the overlapped strips. In this way, the offsets of identical points, features and objects in the overlapped strips could be minimized. Moreover, inspired by the linear features-enhanced 3DCCT, the straight line and planar patch features were also applied as tie features to provide geometrical constraints in the proposed MA process. The use of tie points could reduce or eliminate the relative discrepancies between overlapped strips in the boresight angles and measurements but cannot address which strip should be selected as a reference and cannot identify what corresponding impact on the absolute accuracy of the final merged strip they have. Thus, the use of some type of ground control information is desirable. To remedy this situation, the MA algorithm proposed in this study was achieved by aligning the adjacent strips using both of tie points and tie features. It was designed to minimize the impact of some of the systematic errors in the LiDAR system parameters by improving the compatibility among the overlapping strips. In other words, the offsets of common points, features, and objects from overlapping strips could contain ideal information about the leftover boresight and other systematic errors to refine and improve the mobile LiDAR solution. Moreover, inspired by the utilization of feature constraints developed for 3DCCT, similar straight line and planar patch features were employed in the MA algorithm as the tie features. In comparison with the use of GCPs, this approach is more economic and easily to be made automatically or semi-automatically. Surely, more overlapped data strips will increase the available data volume and measurement redundancy.

In general, assume to have a tie point i with its coordinates $(X,Y,Z)_i^1$ and $(X,Y,Z)_i^2$ in two overlapped LiDAR point clouds, respectively. Straightforward, (1) is applied to model the potential systematic errors with one reasonable simplification that the scale factor may be considered as 1 because the two data strips were collected by the same type of instruments (here, the OpTech LiDAR systems). Mathematically, more than two available tie points result in an overdetermined Least-Squares adjustment system for resolving the parameters. Like the linear feature constraints described in Section 2.1, those characteristic objects can be selected to construct the constraints. The mathematical model given in (2) and (3) along with (1) are integrated together. In practice, the feature constraints are sequentially tested to detect any significant conflict with the tie point measurements processed prior to them. Thus, only the qualified constraints that pass the F-test will be used in the adjustment process. Due to space limit, refer to [Liu, 2015] for more details about the MA algorithmic implementation.

2.3 Post-Processed LiDAR Boresight Calibration using Point Clouds

Indeed, errors can arise from individual sensor calibrations, lack of sensor synchronization and misalignments between the different sensors [Shan and Toth, 2008]. The boresight angle misalignments may never accurately be known but could only be estimated. [Leslar, et al., 2016], for example, presented a successful case study of a dual 2D LiDAR system calibration on a high accuracy test site. Although the proper individual and inter-sensor calibrations are essential, a pre-mission calibration is not always possible due to the lack of a high accuracy test site. Moreover, the lever arms and boresight angles could change over a relatively short time period [Pothou et al., 2009]. Consequentially, any poor system parameter estimates could seriously degrade the accuracy of point cloud by causing certain discrepancies for the common objects among overlapped strips and having an accumulative impact on these strips. It is necessary to compensate for the boresight misalignment in a specific TML system if possible. [Keller et al., 2013] proposed a post-processed boresight calibration of TML systems using linear and/or planar features extracted from two scans acquired during consecutive runs in the opposite driving directions. This calibration process can not only confirm the available boresight angles but also allow further compensation to enhance other quality improvement techniques mentioned above in case the calibrated parameters are significant.

Conceptually, this boresight calibration approach using the acquired LiDAR data was inspired by the calibration procedures for multibeam sonar systems [IHO, 2011]. It is independent of any local behaviour and may significantly enhance the entire refinement process of TML solutions if it is conducted before the

segmental 3DCCT process. Fig. 2 illustrates the geometry of the proposed boresight calibration for the roll (Fig. 2(a)), pitch (Fig. 2(b)) and heading (Fig. 2(c)), respectively. The static objects (e.g., building facades) can be scanned by a TML system from several runs in the opposite directions and variable angular alignment of the laser swath. The boresight angular misalignment ($\Delta\omega$, $\Delta\varphi$, $\Delta\kappa$) between the IMU body frame and LiDAR unit could be modeled as the function of the discrepancies associated with the common targets or objects among the overlapped strips. These misalignments appear with almost every TLS system due to the fact that the axes of the single unit cannot be perfectly aligned, and every mechanical installation implies structural tolerance. Therefore, the poor estimation of boresight angles produces typical errors in the LiDAR point cloud.

A possible roll angle deviation ($\Delta\omega$) could result in a rotation of two scans acquired during consecutive runs in opposite driving directions (Fig. 2(a)). It causes a tilted facade parallel to the driving direction, which was supposed to be vertical. If the first facade tilts toward the vehicle, the second facade shall tilt away from the vehicle. The angle between two mutually tilted surfaces is double the roll angle error between the scanner and IMU with respect to the roll axis in the IMU body frame, i.e., the roll angle error is estimated as:

$$\Delta\omega = -\arccos\left(\vec{n}_1 \cdot \vec{n}_2\right)/2 \quad (1)$$

wherein $\vec{n}_1$ and $\vec{n}_2$ are the unit normal vectors perpendicular to the mutually titled surfaces, respectively. Similarly, an error associated with the pitch angle ($\Delta\varphi$) causes the tilted facade to be perpendicular to the travelling direction (Fig. 2(b)). The facade edge tilts toward the driving direction or oppositely. Then, the angle between the edges of the two facades is double the pitch angle deviation. Thus, one has:

$$\Delta\varphi = \arccos\left(\vec{u}_1 \cdot \vec{u}_2\right)/2 \quad (5)$$

wherein $\vec{u}_1$ and $\vec{u}_2$ are the unit vectors parallel to the corresponding titling straight lines. Furthermore, the residual heading error ($\Delta\kappa$) is estimated through passing by an object in a regular shape (e.g., circle, rectangle) on the ground from the reciprocal travelling directions (Fig. 2(c)):

$$\Delta\kappa = \arctan\left(\Delta x / \Delta L\right) \quad (6)$$

wherein Δx and ΔL are is an offset to the actual position of the object and the distance between the two trajectories from the reciprocal driving directions, respectively.

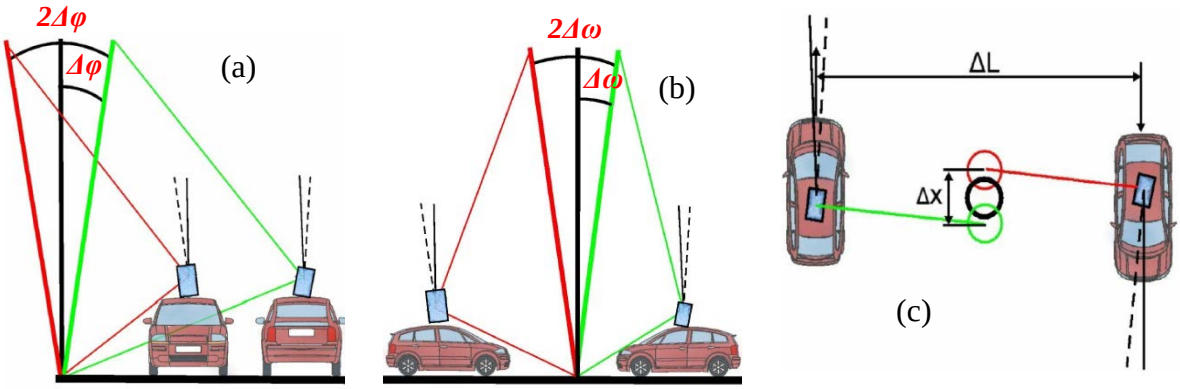

Fig. 2: The field procedures of boresight angles calibration [Keller et al., 2013]. The vehicle passes along the object or facade during consecutive runs in opposite driving directions. (a) Roll, (b) Pitch, (c) Heading.

3. Implementation

As the Linear Features-Enhanced 3DCCT can not only be solely applied to a specific LiDAR point cloud but also integrated into the MA process, its implementation will be explained together with the MA implementation.

3.1 Multistrip Adjustment Process inclusive of Linear Feature-Enhanced 3DCCT

Fig. 3 draws the block diagram of the proposed MA algorithm, which consists of two main steps: 1) the LiDAR point clouds of two overlapped strips are firstly co-registered together using tie points and features, and 2) the linear feature enhanced 3DCCT is further applied to refine the georeference of the whole LiDAR point cloud. It is essential that different features should be applied in the two steps to avoid the reusage of the same features, which may bring a certain unfavorable correlation between the two processing steps. Advantageously, the introduction of more linear tie points and features can practically reduce the number of GCPs.

The right part of Fig. 3 illustrates the software implementation of Linear Features-Enhanced 3DCCT, described in Section 2.1. The available coordinates of GCPs and their corresponding geo-referenced coordinates extracted from the LiDAR point cloud were used as input measurements, which extend the combined least squares method to form a total least-squares method [Wang et al, 2019; Liu, 2015]. Then, a user has two options to select either only GCPs or GCPs with the feature constraints to proceed with the

least squares process. As a standard practice, the τ -test statistic [Caspary, 2000] is implemented to test whether a GCP or a feature constraint is an outlier or not. Besides, the *F*-test statistic is constructed to test the consistency among all the observations. The variance components for the available GCP coordinates and the extracted coordinates from the LiDAR solution were then estimated to iterate the Least-Squares process. Finally, the accuracies of the LiDAR solutions before and after the adjustment were assessed using the extra GCPs that were not used in the 3DCCT process.

3.2 Post-Processed LiDAR Boresight Calibration using Point Clouds

The processing flow for conducting the proposed boresight calibration in post-processing (Refer to Section 2.3) is given in Fig. 4. The implementation consists of two modules: without calibration on the left and with calibration on the right. For the proposed calibration, the identified facade objects or sections with different spatial orientations are extracted and taken to estimate the deviation of boresight angles individually. Specifically, estimating the errors in roll and pitch requires the facades to be parallel (e.g., building roofs and windows along the road) with and perpendicular (e.g., traffic lights and signs) to the travelling directions, respectively. The residual error in heading is estimated by driving through the objects with the regular shapes (e.g., pavement marking, sewer and sidewalk curb) on the ground. Then, the raw point cloud data are re-processed by applying the calibrated boresight angles. After that, the linear feature-enhanced 3DCCT is introduced in the single strip, and then the MA approach with two strips can be introduced by applying both the original LiDAR data and the corrected mobile LiDAR data for the calibrated boresight angular biases.

Technically, each estimated boresight error should be significant to make fair compensation. In relation to the typical 2-3cm accuracy with the direct-georeferencing trajectory according to the SBET (Smoothed Best Estimated Trajectory) solution, the corresponding estimate of boresight errors should be about 0.005°. Furthermore, the proposed approach requires sufficient planar features with different spatial orientations, which could be easily identified in the urban or sub-urban regions, where an adequate amount of facade sections, roofs of buildings, traffic signs and pavement markings along the street containing preferably flat surfaces of variable orientation are available. Obstructions of GPS signals can also significantly degrade the accuracy of position and attitude information. So, one needs to carefully screen the data to find adequate subareas for carrying out such calibration.

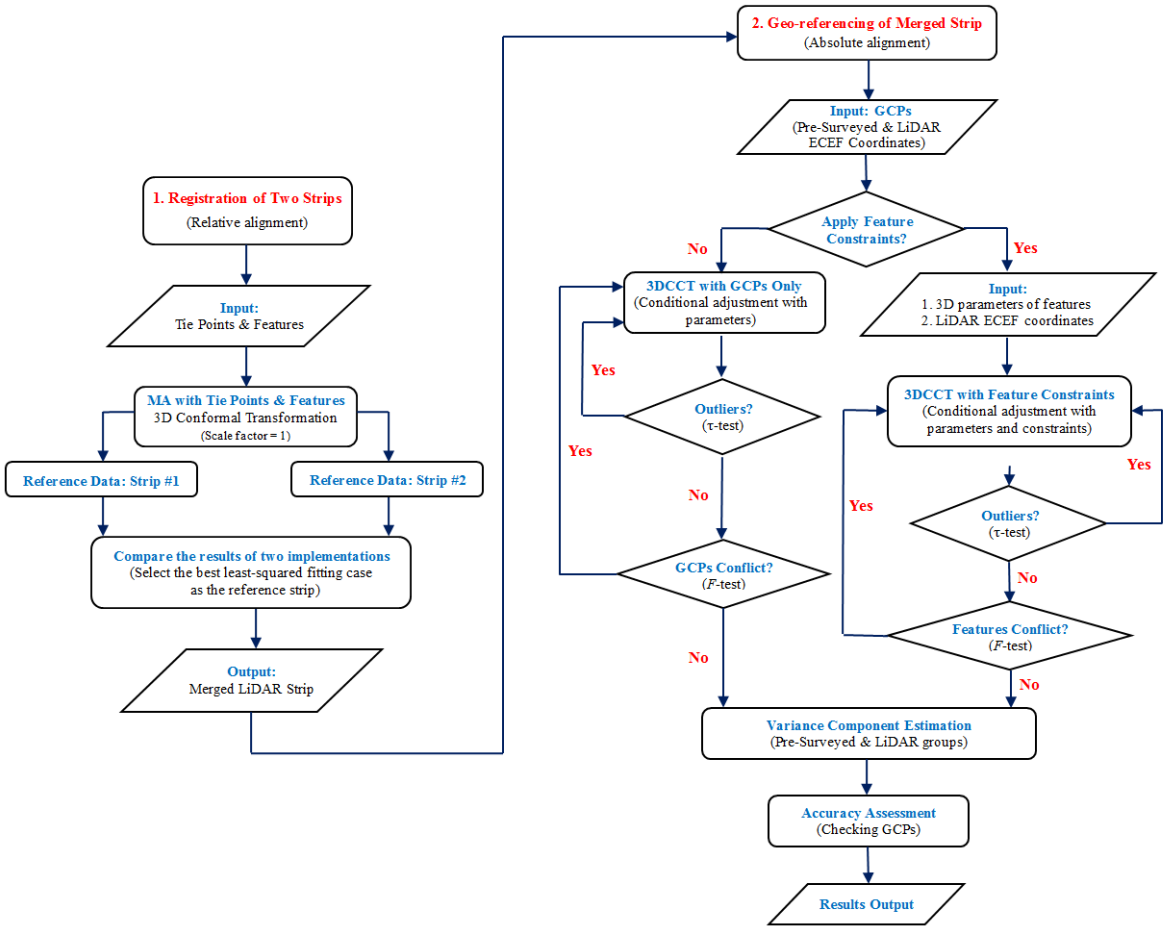

Fig. 3 Flowchart of Multistrip Adjustment Process

4. Test Data and Results

The Optech Lynx Mobile Mapper V200 was used to acquire the raw TML data. An overview of its technical specifications is given in Table 1. A relative complex testing site lopped around the Black Creek Pioneer Village, extended to the east on Shoreham Drive on the North of Aviva Tennis Center to the Calumet Residence on Keele Campus of York University (Fig. 5), which is less than 2.5km away from the Optech GPS base station that served the entire data acquisition. The mobile LiDAR data acquisition was focused on the two highlighted areas labelled as Area #1 and Area #2 in Fig. 5. First, multiple strips of LiDAR data at PRF of 250kHz and mirror rate of 200Hz were recorded in both opposite directions, of which the data analysis and their results from strips 012 (forward), 013 (reverse), 014 (forward) and 015 (reverse) were presented in this work.

To apply the proposed techniques, 3D control networks relative to the Optech GPS base station were established in the working area using GPS baselines and more GPCs were further densified either on-ground or off ground through 3D intersection with 3 agreed full observation sets on the base of their control networks using Leica TC1800 total stations (1σ: ±1" H&V angles and ±(1mm+2ppm) (range)).

4.1 Test Data

The data was split into two labelled areas to serve different testing purposes:

Table 1: Overview of Technical Specification (OpTech Inc, 2012)

Parameter	Optech Lynx V200
Number of LiDAR	2
Camera support	Up to 2 cameras
Maximum range	200m, 20%
Range precision	8mm, 1σ (Under test conditions)
Absolute accuracy	±5cm, 1σ (Under test conditions)
Laser measurement rate	75 – 500kHz programmable
Measurement per laser pulse	Up to 4 simultaneous
Scan frequency	80 – 200 Hz programmable
Scanner field of view	360° without obscurations
Operating temperature	-10 °C to +40°C (extended range available)
Storage temperature	-40°C to +60°C
Laser classification	IEC/CDRH Class 1 eye-safe

Area #1 (Fig. 5 and 6): A stretch of Shoreham Drive between Calumet Resident and Canada Tennis Center (a little west beyond the Ian Macdonald Blvd (ca. 230m), designed to validate the algorithms and strategies under an ideal condition, i.e., in a relatively small area with adequate ground control points and feature constraints. The data acquisition was conducted mostly at a low speed of 20km/h (ca. 5.6m/s, maximum up to 13m/s). The accuracy of the direct-georeferencing (POS SBET) was better than ±1.5cm horizontally and ±3cm vertically. A GPS baseline control network was established with seven GCPs at its 3D accuracy between ±3.3 and ±4.0mm. Further, two types of the 76 existing characteristic points at the scene (22 pavement markings, curbs etc., on the ground and 54 corners of artificial objects, guide boards, traffic lights and signs, etc. off the ground were selected as GCPs (Fig. 7), from which 4 horizontal and 6 vertical feature constraints were generated in addition (Fig.8). The distribution of the used GCPs and features are plotted in Fig. 9 and 10.

Area #2 (Fig. 5 and 12): A street loop (ca. 2.35km) was selected to test the proposed strategies under real environmental conditions with a speed limit of 40km/h - 60km/h on different streets. The accuracy of the SBET solution of the trajectory was similar to the solution in Area #1. A static baseline on the loop was linked to the same GPS base station, under which 135 GCPs (Segment East: 46; Segment North: 18; Segment West: 24; Segment South: 47) were established on both sides of the streets along the path using rapid static and stop-and-go GPS approach (Fig. 13). Their usage is given in Fig. 14. The performance of the proposed techniques was analysed through six different GPC usages: every 25m, 50m, 75m, 100m, 150m and 200m (Fig. 15).

4.2 Results and Analysis

Despite multitudes of our strategic studies about how to utilize three techniques in practice, it is impossible to present all the studied scenarios due to the space limit. From the technical., practical., and end-user implementable aspects, we focus on three scenarios: 1) GCP usage optimization, 2) Multitrip adjustment (i.e. co-registration of overlapped strips and linear feature enhanced 3DCCT (Fig. 3), and 3) Combination and comparison of the linear feature enhanced 3DCCT (single trip) and MA with and without post-processed LiDAR boresight calibration. For the details of other scenarios mentioned above, refer to [Hu et al., 2012; Liu, 2015; Leslar, 2016].

4.2.1 GCP Usage Optimization

Under consideration of how to reduce the cost associated with the GCP establishment, the optimal density of the ground control points was investigated in terms of the efficiency and cost-effectiveness using test data in Area #2 (long data strips and realistic field environment). By applying the 3DCCT to single strip data directly with having a maximum of 135 GCPs in total, the accuracy performance was compared among different GCP usages in terms of six different GCP separations from 25m to 200m (i.e.,

25m, 50m, 75m, 100m, 150m and 200m) using the 59 checking GCPs (Fig. 15 and 16).

The RMS accuracies of the original LiDAR point cloud were ±3.5cm (horizontal) and ±4.2cm (vertical). Among all the scenarios, the lowest RMS of ±1.3cm (horizontal) and ±1.2cm (vertical) were at the GCP separation of 25m. The vertical RMS was ±1.2cm at the GCP separations of 50m and 75m, whilst the corresponding horizontal RMS were ±1.4cm and ±1.5cm, respectively. At the GCP separation of 100m, the RMS values were ±1.6cm horizontally and ±1.3cm vertically. Overall, the performance was not degraded significantly as the GCP separation was enlarged from 25m to 100m. Furthermore, at the GCP separation of 150m, the resulting vertical RMS was ±1.6cm; however, the horizontal RMS was decreased down to ±1.9cm. The horizontal RMS went further down to ±2.1cm at the GCP separation of 200m. Clearly, the accuracies from the last two scenarios were significantly decreased.

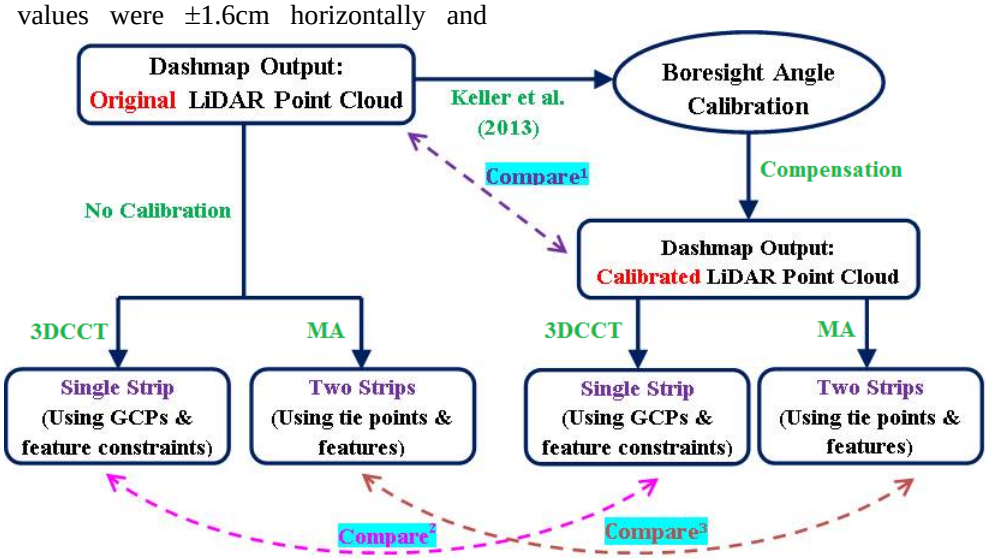

Fig. 4: Flowchart of the Post-Processed Boresight Calibration.

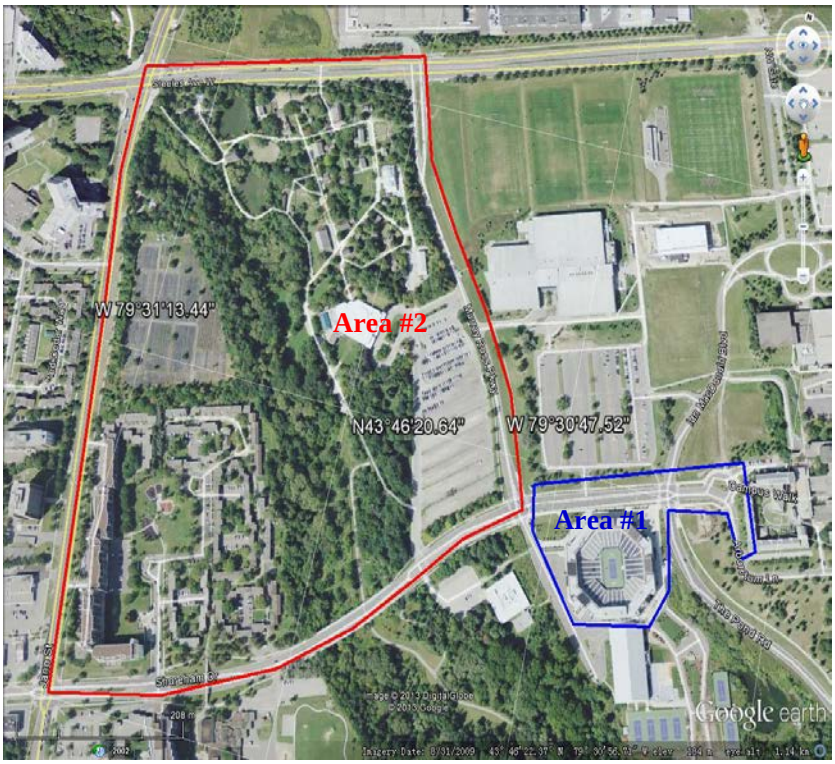

Fig. 5: Location of Black Creek Pioneer Village in Toronto, Canada (Area #1 (blue): A stretch of Shoreham Drive from Calumet Resident to the west and Area #2 (red): the street loop from Steeles Ave W., Murray Ross Pkwy, Shoreham Dr., Jane St. and back to Steeles Ave. W.)

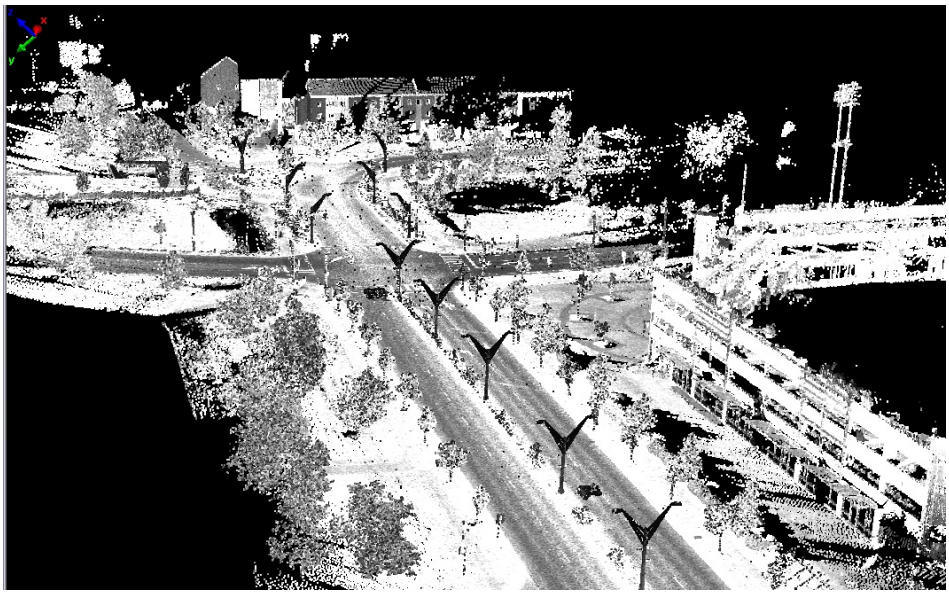

Fig. 6: Overview of Area #1 (Laser PRF:250kHz and mirror speed: 200Hz)

Fig. 7 Examples of Two types of the selected control points and features (a) on the ground and (b) off ground

Fig. 8 Examples of horizontal and vertical directional feature constraints

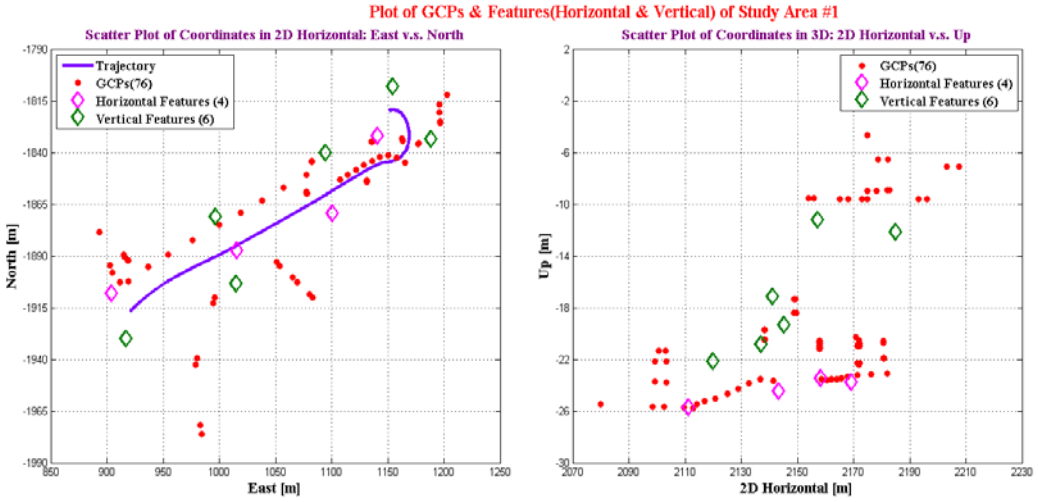

Fig. 9 Scatter plot of 76 GCPs and 10 feature constraints in Area #1

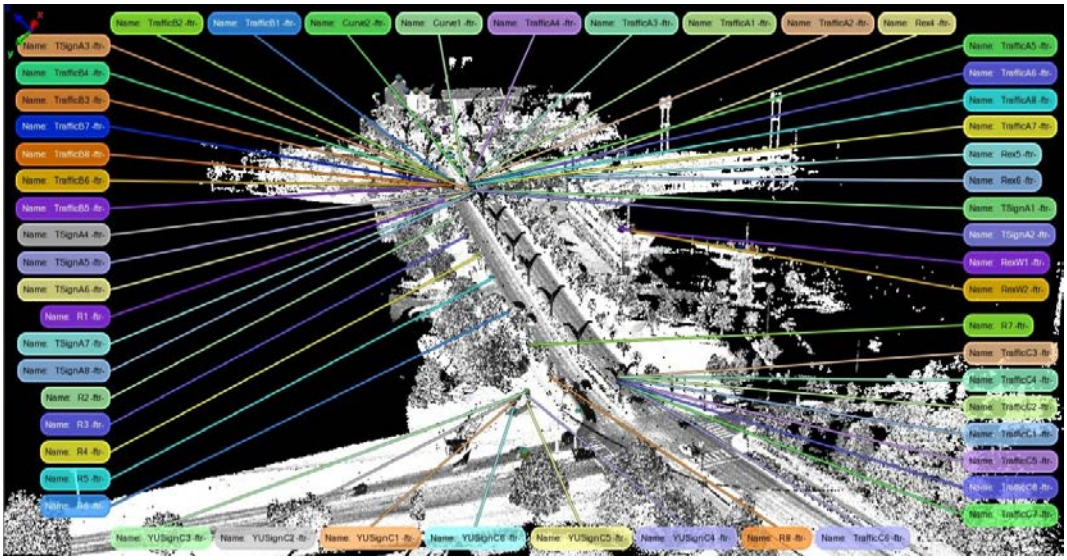

Fig. 10 Overview of the distribution of 76 control points over the 200m

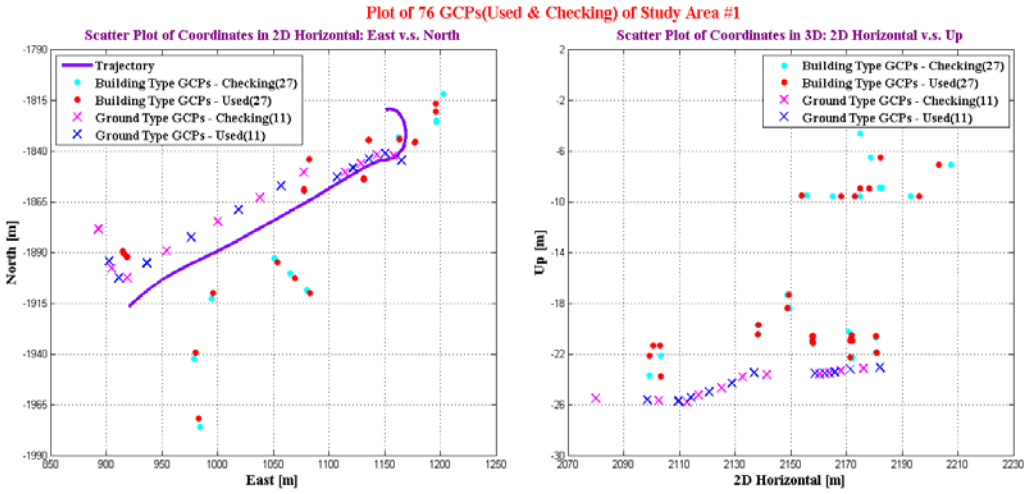

Fig. 11 Scatter plot of 76 GCP: used and checking, in Area #1

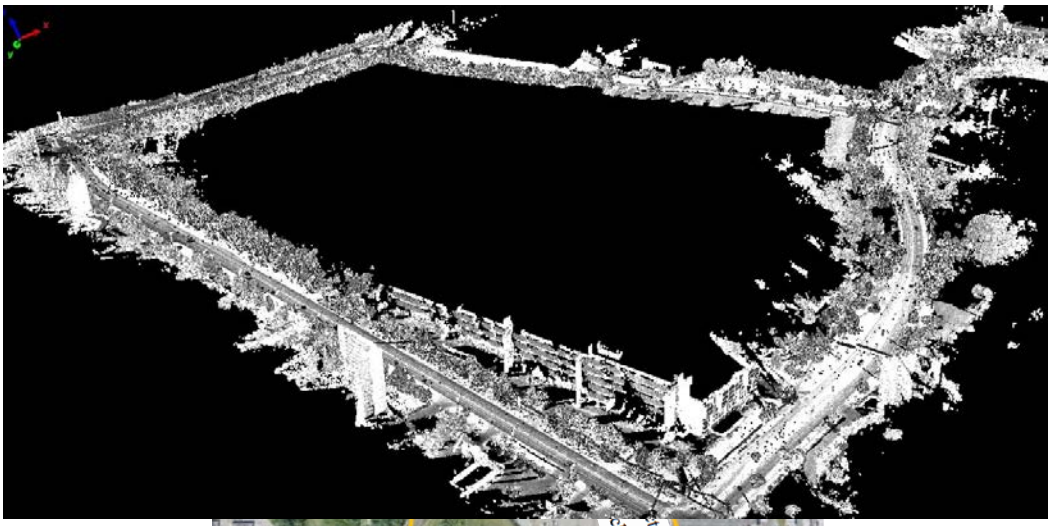

Fig. 12: Overview of Area #2 (Laser PRF: 250 kHz and mirror speed: 200 Hz).

Fig. 13: Overview of Control Network with all the GCPS using the marked road curbs with the separation of a few meters up to 50m (rapid static and stop-and-go, 5min stop on each) in Area #2 (mission 1 in red and mission 2 in blue, each with using the average coordinates after their own double-run observation)

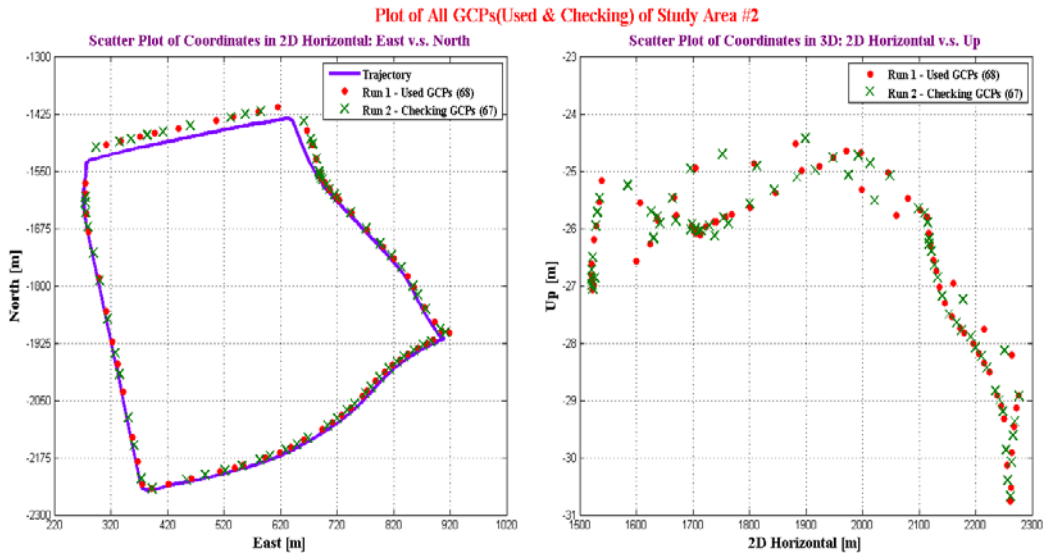

Fig. 14: Scatter plot of 135 GCPs (65 used in data improvement process (red); 67 used for checking (green))

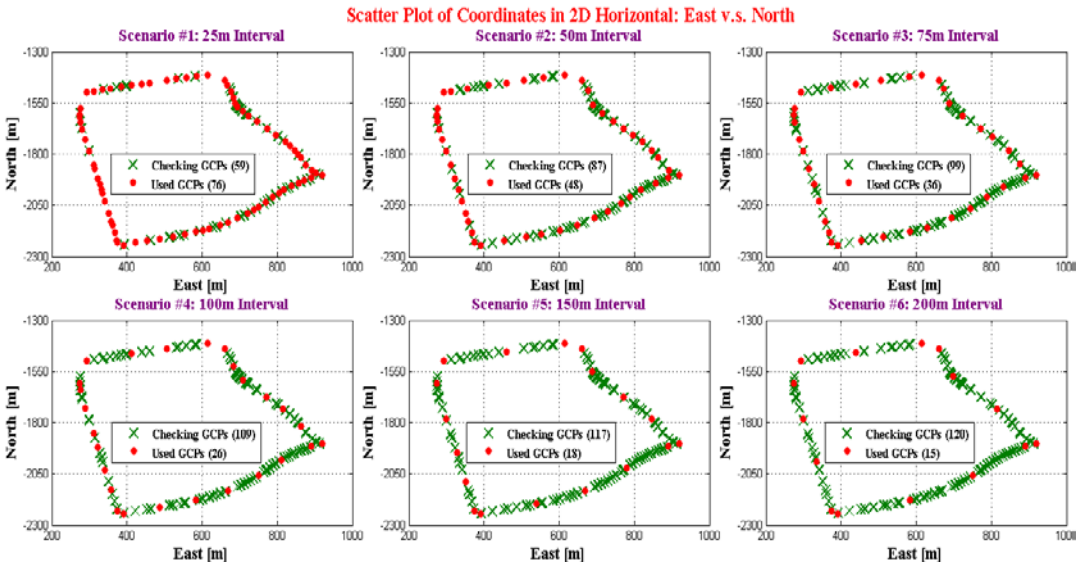

Fig. 15: Horizontal scatter plot of the GCPs for six scenarios (separation of 25m, 50m, 75m, 100m, 150m and 200m)

Expectedly, the smaller the GCP separation (i.e., more GCPs) is, the more accuracy improvement is achieved through the 3DCCT. However, the overall accuracy was not degraded very significant (e.g., 5mm horizontally) from 50m, 75m to 100m specifically with the test data (Area #2). That is, there will be no more significant accuracy gain once the number of the GCPs is increased to a certain level, especially vertically. Noteworthily, the above improvement can be further enhanced by adding linear features that could further reduce the number of the GCPs. It is suggested that 100m separation for GCPs should be followed loosely in practice as more GCPs may be necessary locally in case one more poorly performed SBET sections occur, and a local refinement is even required. This is essential to optimally select the GCPs after the project budget and accuracy requirements.

Similar outcomes were also concluded from the similar analysis of Area #1.

4.2.2 Multistrip Adjustment

Regarding applying the multistrip adjustment for quality improvement of TML data, three particulars need to be practically considered. **First**, as the TML point clouds are georeferenced, the co-registration of multiple strips does not usually require any GCPs. **Second**, if the data strips are acquired from the same system in relatively recent times, the scale factor may not be involved in their co-registration. **Third**, no linear feature enhanced 3DCCT may be needed in any data patch prior to the MA if no significant patchwise GNSS outages occur in the GNSS/IMU integrated SBET solution (i.e., partially with significantly unsatisfactory SBET solution). Fortunately, the multiple strips of data acquired in Area #1 and Area #2 do satisfy the particular conditions mentioned above. Hence, they were directly co-registered by following the flow given in Fig. 3. The strips 12, 13 and 14 in Area #1 were selected to test out the MA process.

To align two strips relatively, 52 tie points and 23 tie features were used in Area #1. As an example, Fig. 17 presents a merged scene around the Calumet Residence from strips 12, 13 and 14 in Area #1. From the POS LV420, the position accuracy (1σ) of its SBET solution was better than ±1.5cm horizontally for all three strips and between ±3cm and ±3.7cm vertically, specifically, around ±3.5cm vertically for strip 13, lower than the other two strips. Further, half of the GCPs (38) participated in the feature enhanced 3DCCT with the co-registered dual strip data as the other half (also 38) were used as the performance checking points (Fig. 11).

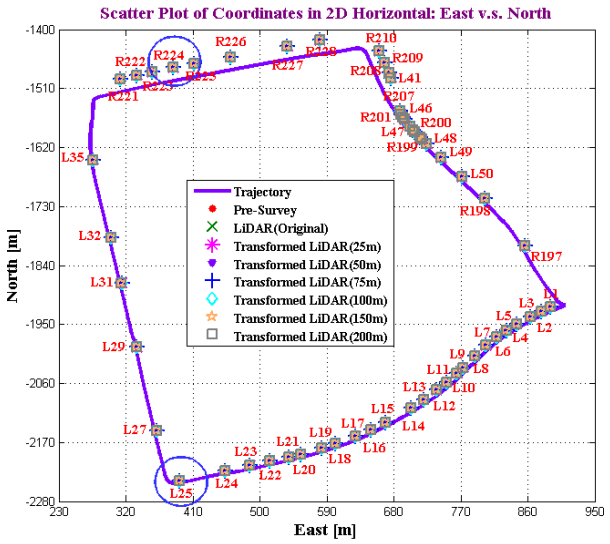

Fig. 16: Scatter plot of 59 Checking GCPs in Area #2

Table 2 presents the errors and RMS in detail through the 38 checking GCPs in Area 1. In summary,

the RMS error of the original LiDAR solution based on errors calculated against the 38 checking GCPs were ±5.0cm horizontally and ±3.9cm vertically. The refined single strip solution was improved up to ±2.3cm horizontally and ±1.8cm vertically. After the multistrip adjustment with two strips driven in the same direction (strips 12 & 14), the horizontal accuracy was only improved to ±2.2cm, with two strips collected in the opposite driving directions, the accuracies were further increased to ±2.0cm horizontally and ±1.6cm vertically.

In general, the performance analysis concluded that the multistrip adjustment process could further improve the quality of LiDAR data, especially, reaching the best accuracy improvement using strips collected in opposite driving directions. In addition, the same technique applied to the co-registered strips (acquired in the opposite driving directions) resulted in the RMS of ±2.2cm horizontally and ±1.8cm vertically by only using 16 GCPs, which performed equivalently to the single strip scenario by using 38 GCPs. Hence, the multistrip adjustment (MA) process could effectively enhance the accuracy improvement of TML solutions even with the significantly reduced number of GCPs.

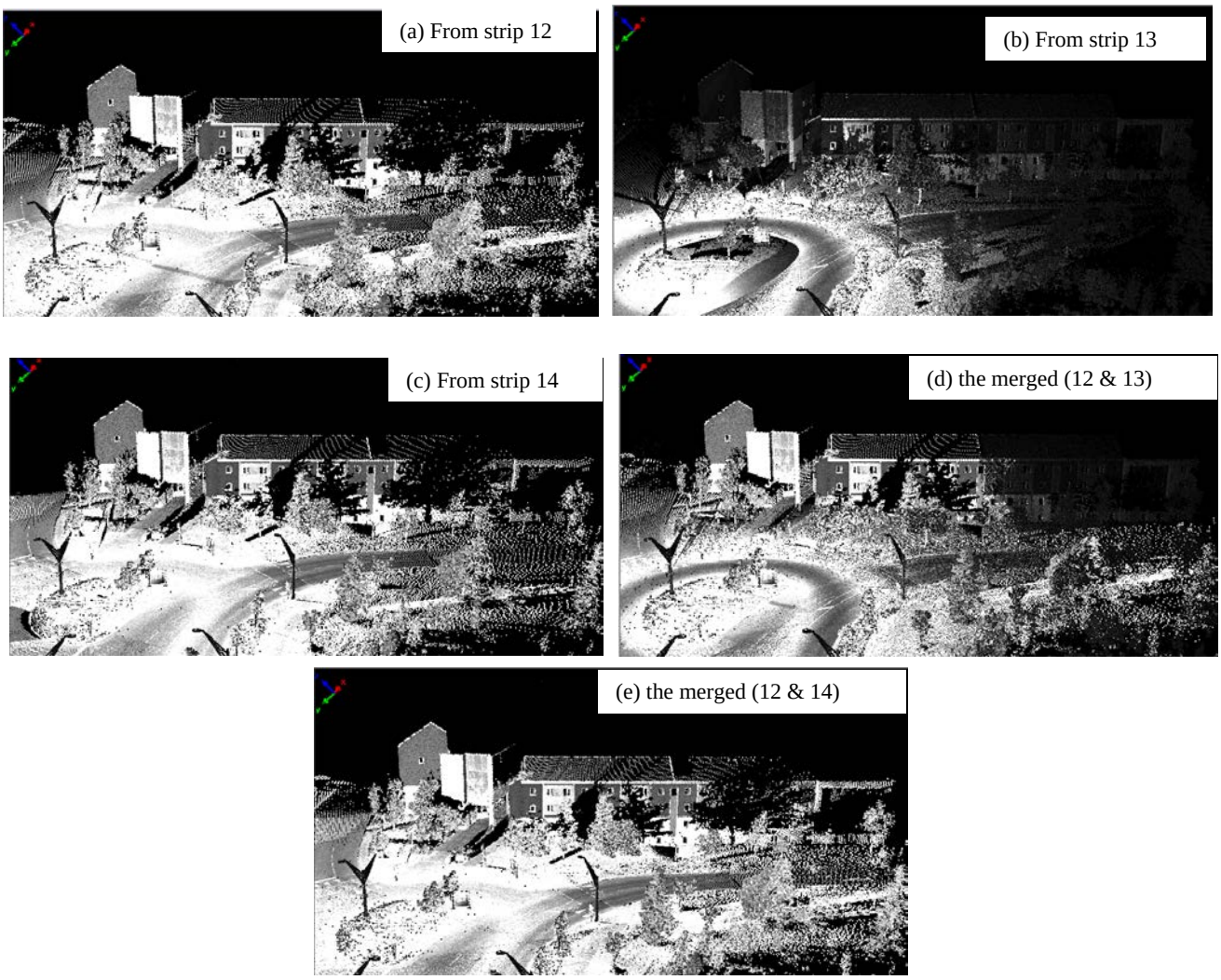

Fig. 17: An example of the merged patch: a LiDAR scanned scene around Calumet Resident (Area #1): (a) strip 12 (forward); (b) strip 13 (reverse), (c) strip 14 (forward), (d) the merged (strips 12 & 13) and (e) the merged (strips 12 & 14).

4.2.3 Quality Improvement with the aid of Preliminary Post-Processed Boresight Calibration

This section is focused on the results from the application of preliminary boresight calibration with MA (feature enhanced 3DCCT inclusive).

First, an attempt at estimating the boresight misalignment was carried out. A certain number of the facade objects or sections, spatially oriented differently, need to be extracted to estimate the boresight errors. With respect to the vehicle's driving direction, the parallel facades, e.g., building roofs and windows along the road are used to determine the error in roll angle, while the perpendicular ones, e.g., traffic lights and signs, are used to estimate the error in the pitch angle. The error in the heading angle is estimated by driving through the objects with regular shapes, e.g., pavement marking, sewer and sidewalk curbs, on the ground. Then, the raw point clouds will

be corrected by applying the calibrated boresight angular errors. As strips 12 and 13 were consecutively acquired by passing the scene from two opposite directions, they satisfy our need here. Second, the corrected raw point clouds will be further refined using the feature enhanced 3DCCT and the MA approach. In the end, the solutions resulted from different scenarios will be compared to make realistic conclusions.

With both datasets, 20 facade objects spatially oriented differently were chosen to calibrate the errors in boresight angles individually, which are listed in Table 3 below. Clearly, they were relatively

Table 3: The calibrated boresight angular errors

	Area 1		Area 2	
LiDAR #	1	2	1	2
Roll (˚)	-0.013	0.008	-0.012	0.010
Pitch (˚)	0.033	-0.026	0.024	-0.028
Heading (˚)	-0.005	-0.006	-0.008	-0.005

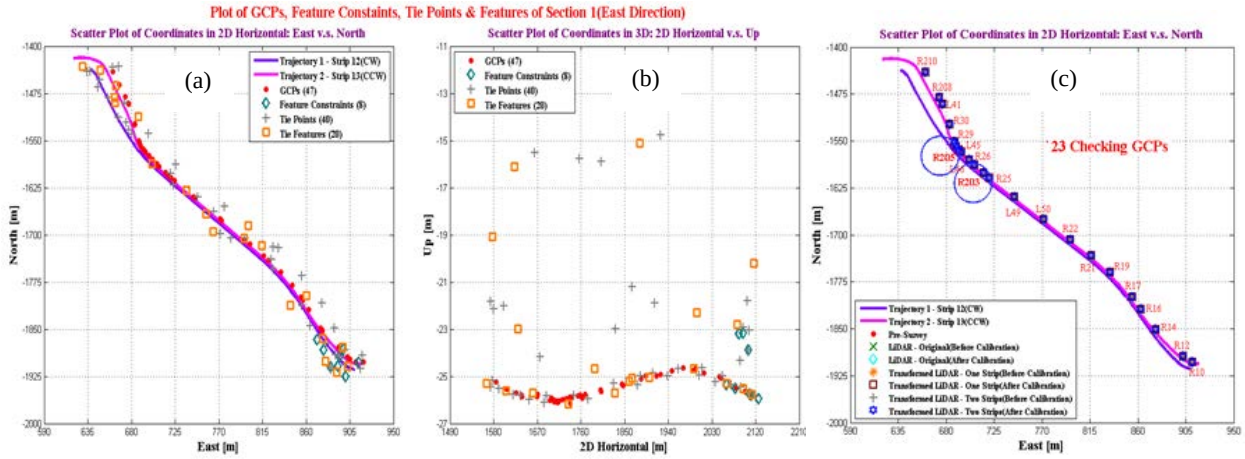

Fig. 18: Scatter plot of the selected segment in Area 2 (ca. 570m)

significant and agreed with each other as well.

The east side segment of strips 12 and 13 along Murray Ross Pkwy in Area 2 is selected to proceed with our analysis in this subsection (Fig. 18). 40 tie points and 20 features were used in strip co-registration whilst 24 GCPs and 8 features were applied in 3DCCT and 23 checking GCPs were included to conduct performance analysis.

Through all the 23 checking GCPs in the east segment (Area 2), an error analysis of different LiDAR data refinement strategies is given in Table 3. The compensation effect using the calibrated boresight errors (Case 1 vs. Case 2) appeared very clearly in Table 3 as the difference between the single strip (Case 3) and two-strip refinements (Case 4) after the compensation for the boresight errors was indistinct. Although the effect of a boresight calibration depends on how significant the errors are, it could improve the data quality and reliability overall. That is, it can be used to verify the boresight angles and may also further compensate for significant boresight errors.

As a result, either one of the two following strategic combinations may be chosen in an efficient and cost-effective way in the conditions of a TML data acquisition:

- **Strategy 1**: perform the preliminary post-processed boresight calibration and then apply the feature-enhanced 3DCCT to the single strip data.
- **Strategy 2**: directly apply the MA technique to the overlapped data strips (without the preliminary post-processed boresight calibration). After the overlapped strips are co-registered, conduct a feature enhanced 3DCCT adjustment to the entire LiDAR data.

5. Conclusions and Remarks

To comprehensively improve the solution quality of TML systems in Engineering Surveys, this manuscript proposed and stutied three techniques: (1) Linear feature-enhanced 3DCCT; (2) Multistrip Adjustment, and (3) Preliminary Post-Processing LiDAR Boresight Erro Calibration. Through two relatively large scale of real datasets, they were implenented, and their performance per various different scenarios was compared. Three essential studies have been detailed to show their performance in reality: (1) Usgae Optimization of GCPs in 3DCCT; (2) Performance of multistrip adjusment and the comparison with single strip refinement, and (3) Quality Improvement with the aid of post-processed boresight calibration. The outcomes from the real test datasets are very convincing and possess high potential to be applied to Engineering Surveys.

Fig. 19 outlines a practical post-processing protocol for efficient and cost-effective accuracy improvement of TML solutions using the proposed techniques.

Next, our team may focus on two specific tasks: (1) develop more economical, automatic, or semi-automatic methods to identify distinct GCPs, linear feature constraints, and tie points and tie features; (2) Further study how to refine mobile LiDAR data with poor local direct-georeferencing SBET, specifically try the dynamic network technique to overcome the negative impact of GNSS gaps on direct georeferencing.

6. Acknowledgement

The research was partially funded by MTO HIIFP (Highway Infrastructure Innovation Funding Program) and NSERC. The authors acknowledge the support of LiDAR data acquisition from Optech Inc., Canada. Not the last, we gratefully acknowledge the contribution made by the individuals of the Earth Observation Laboratory of York University.

7. Reference

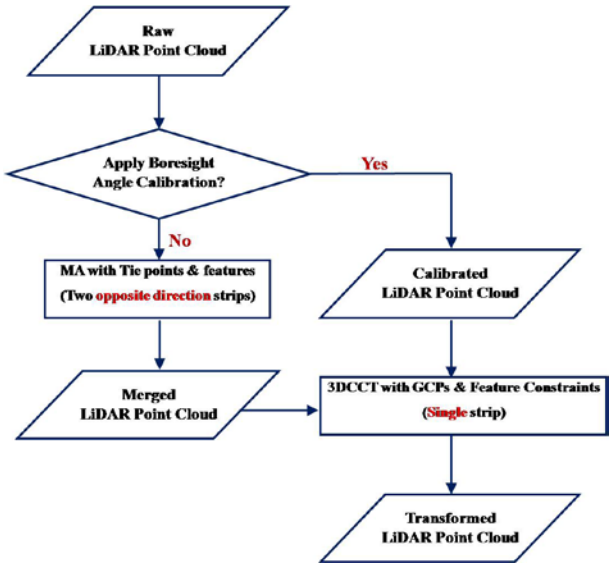

Fig. 19: Practical Post-Processing Protocol for Accuracy Improvement of Terrestrial Mobile LiDAR solutions

Bali, Vinayak (2023): Terrestrial Mobile LiDAR Market Report 2023, Cognitive Market Research, https://www.cognitivemarketresearch.com, 2023.

Bretar F., Pierrot-Deseilligny M. and Roux M. (2004): Solving the Strip Adjustment Problem of 3D Airborne LiDAR Data. Geoscience and Remote Sensing Symposium, Proceedings of the IEEE IGARSS'04, Alaska, vol 7, pp. 4734 - 4737.

Caspary, Williams (2000): Concepts of Network and Deformation Analysis, Monograph 11, School of Geomatic Engineering, UNSW, Australia, 2000.

Chen, Hui-Peng; Kuan-Tsung Chang and Jing-King Liu (2012): Strip Adjustment of Airborne LiDAR Using Ground Points, 33rd Asian Conference on Remote Sensing, Thailand, 2012

Crombaghs, M., E. De Min and R. Bruegelmann (2000): On the Adjustment of Overlapping Strips of Laser Altimeter Height Data. International Archives of Photogrammetry and Remote Sensing, 33(B3/1): 230-237.

Di Stefanoa, F.; S. Chiappinib; A. Gorrejaa; M. Balestrab and R. Pierdicca (2021): Mobile 3D scan LiDAR: a literature review, Geomatics, Natural Hazards and Risk, 2021, Vol. 12, No. 1, 2387 – 2429.

Durrieu, S., Allouis, T., Fournier, R., Véga, C. and Albrech, L. (2008): Spatial Quantification of Vegetation Density from Terrestrial Laser Scanner Data for Characterization of 3D Forest Structure at Plot Level. SilviLaser 2008, Sept. 17-19, Edinburgh, UK, pp. 325-334.

Elsayed, Hamdy and Ahmed Shaker (2023): From Stationary to Mobile: Unleashing the Full Potential of Terrestrial LiDAR through Sensor Integration, Canadian Journal of Remote Sensing, Vol. 49, No.1, 2023.

Esfandabadi, Alireza S. (2018): Highway Cross Slope Measurement Using Airborne and Mobile LiDAR, PhD dissertation, Clemson University, 2018.

EST (*E*ngineering *S*urveys *T*oronto) (2010): Engineering Survey Standards for Consultants, Version 2.5, Technical Services, Survey & Mapping Services, Engineering Surveys Toronto, 2010, www.toronto.ca/wp-content/uploads/2017/11/.

Filin, S. (2003): Analysis and Implementation of a Laser Strip Adjustment Model, International Archives of Photogrammetry and Remote Sensing, 34 (Part 3/W13): 65–70.

Glennie, C., (2007): Rigorous 3D error analysis of kinematic scanning LIDAR systems, Journal of Applied Geodesy, 1 (2007), 147–157.

Glennie, C. (2009): Kinematic terrestrial light-detection and ranging system for scanning, Transportation Research Record, 2105, 135–141.

Glennie, Craig; Kresimir Kusevic and Paul Mrstik (2006): Performance Analysis of a Kinematic Terrestrial LiDAR Scanning System, MAPPS/ASPRS 2006 Fall Conference, Texas, 2006.

GRÄFE, G. (2008): Kinematic 3D Laser Scanning for Road or Railway Construction Surveys, 1st International Conference on Machine Control and Guidance 2008.

Guan, Haiyan; Jonathan Li; Shuang Cao and Yongtao Yu (2016): Use of mobile LiDAR in road information inventory: a review, International Journal of Image and Data Fusion, Vol. 7, No. 3, 219 – 242, 2016.

Table 2: The summary of the errors against the 38 checking CGPs from (i) the ***original*** point cloud, refined solutions through (ii) the feature enhanced 3DCCT using a single strip, (iii & iv) the MA process using two strips acquired in the opposite driving directions and in the same direction, respectively (Area #1).

No.	**ID**	**Case 1: Original (strip 12) [cm]**					**Case 2: Singe Strip (strip 12) [cm]**					**Case 3: Opposite Direction Strips [cm]**					**Case 4: Same Direction Strips [cm]**				
		N	E	U	2D	3D	N	E	U	2D	3D	N	E	U	2D	3D	N	E	U	2D	3D
1	Rex2	1.35	-2.58	6.55	2.91	7.17	0.45	0.78	1.22	0.90	1.52	0.55	-0.77	0.87	0.95	1.29	0.77	-0.85	0.93	1.15	1.48
2	Rex4	-2.20	-1.52	6.32	2.67	6.86	0.41	-0.97	1.22	1.05	1.61	-0.38	-0.79	0.67	0.88	1.10	-0.68	-1.56	0.67	1.70	1.83
3	Rex6	1.12	0.53	6.65	1.24	6.76	0.64	0.27	0.79	0.69	1.05	0.79	0.66	0.74	1.03	1.27	0.45	0.34	0.29	0.56	0.63
4	TrafficA3	-2.45	1.13	4.73	2.70	5.45	-0.89	0.90	-0.93	1.27	1.57	-0.47	0.93	-1.76	1.04	2.05	-0.79	0.39	-1.67	0.88	1.89
5	TrafficA7	1.24	1.66	5.54	2.07	5.91	0.56	1.42	0.93	1.53	1.79	0.56	0.69	0.73	0.89	1.15	0.86	1.44	0.69	1.68	1.81
6	SWTraffic	1.03	0.53	6.26	1.16	6.37	0.22	0.36	-0.23	0.42	0.48	0.66	0.82	-1.53	1.05	1.86	0.67	0.96	-0.64	1.17	1.33
7	S̄WTraffic	2.23	-2.34	3.34	3.23	4.65	0.55	-0.76	0.63	0.94	1.13	0.48	-0.45	-0.55	0.66	0.86	0.88	-0.45	-0.62	0.99	1.17
8	ẎUSignA2	-2.74	-2.65	6.24	3.81	7.31	-0.75	-0.99	-0.82	1.24	1.49	-0.37	-0.71	-0.87	0.80	1.18	-0.45	-0.63	-0.45	0.77	0.90
9	YUSignA4	1.05	-3.71	4.74	3.86	6.11	1.04	-1.15	-1.31	1.55	2.03	0.51	-0.73	-0.93	0.89	1.29	1.16	-0.83	-1.34	1.43	1.96
10	YUSignA7	-2.70	-0.39	5.84	2.73	6.45	-0.69	-0.85	-1.21	1.09	1.63	-0.36	-0.78	-0.63	0.86	1.07	-1.67	-1.32	-1.04	2.13	2.37
11	YUMap1	0.62	-3.86	4.15	3.91	5.70	0.24	1.33	-0.98	1.35	1.67	0.97	1.01	-0.57	1.40	1.51	1.45	-1.25	-0.78	1.91	2.07
12	YUMap2	0.56	-3.36	5.36	3.41	6.35	0.17	0.78	-1.88	0.80	2.04	0.68	-0.83	-1.33	1.07	1.71	0.77	-0.29	-1.86	0.82	2.03
13	YUMap6	2.40	2.76	5.59	3.66	6.68	2.03	1.23	-1.64	2.37	2.89	1.49	-1.14	-1.69	1.88	2.53	0.73	-1.22	-1.24	1.42	1.89
14	StopSign3	0.21	0.00	3.33	0.21	3.34	0.09	-0.35	-3.03	0.36	3.05	0.73	-0.34	-1.89	0.81	2.05	0.69	-0.58	-2.02	0.90	2.21
15	StopSign4	0.57	-2.51	6.10	2.57	6.62	0.46	-0.86	0.25	0.98	1.01	0.85	-0.79	0.56	1.16	1.29	0.74	-0.75	0.56	1.05	1.19
16	StopSign6	0.96	-3.62	6.45	3.75	7.46	0.84	-0.97	0.59	1.28	1.41	0.95	-1.43	0.61	1.72	1.82	0.44	-1.11	0.33	1.19	1.24
17	StopSign8	-2.23	-2.71	6.50	3.51	7.39	1.43	-0.98	0.64	1.73	1.85	-1.05	-0.86	0.83	1.36	1.59	-1.73	-1.33	1.41	2.18	2.60
18	Building1	-2.88	-2.23	5.53	3.64	6.62	-1.37	-1.56	0.29	2.08	2.10	-1.31	-1.34	0.61	1.87	1.97	-1.45	-1.45	0.75	2.05	2.18
19	Building4	-2.23	1.37	5.06	2.62	5.70	-1.93	0.94	0.73	2.15	2.27	-1.39	0.42	0.33	1.45	1.49	-1.58	0.68	0.44	1.72	1.78
20	Building5	-2.13	2.03	5.83	2.94	6.53	1.83	1.59	0.75	2.42	2.54	0.83	0.97	1.27	1.28	1.80	1.48	1.56	1.73	2.15	2.76
21	YUSignB1	2.41	1.64	6.61	2.92	7.22	0.13	0.98	-0.48	0.99	1.10	-0.69	1.34	-0.45	1.51	1.57	0.78	1.22	-0.33	1.45	1.49
22	YUSignB3	0.61	0.63	6.20	0.88	6.26	-0.79	0.36	1.16	0.87	1.45	-0.45	0.79	0.55	0.91	1.06	-0.88	0.39	0.67	0.96	1.17
23	RexW2	-3.67	3.32	-4.05	4.95	6.39	-0.42	0.84	-0.27	0.94	0.98	-0.57	0.72	-0.93	0.92	1.31	-0.93	0.52	-1.23	1.07	1.63
24	RexW4	-4.20	0.39	6.39	4.22	7.66	-1.02	0.57	0.79	1.17	1.41	-1.23	0.68	1.14	1.41	1.81	-0.66	0.64	0.96	0.92	1.33
25	RexW6	-2.23	-2.06	3.48	3.04	4.62	-0.68	-0.86	-0.79	1.10	1.35	-1.34	-0.86	0.99	1.59	1.87	-0.85	0.77	1.37	1.15	1.79
26	YUSignC4	-2.59	-1.19	6.59	2.85	7.18	-0.48	-1.58	0.74	1.65	1.81	-1.14	1.49	-0.69	1.88	2.00	-1.09	0.55	-0.56	1.22	1.34
27	YUSignC6	-2.23	-4.16	5.88	4.72	7.54	-1.00	-0.99	-1.08	1.41	1.77	-0.99	-0.71	1.56	1.22	1.98	-0.65	-0.79	1.35	1.02	1.69
28	Curve2	-0.78	-2.27	6.16	2.40	6.61	-0.89	-0.71	-0.84	1.14	1.41	-0.66	-0.77	-0.74	1.01	1.26	-0.98	-0.74	-0.67	1.23	1.40
29	Curve4	1.63	-3.90	5.59	4.23	7.01	-0.67	-0.89	-0.78	1.11	1.36	-0.45	-0.82	-0.52	0.94	1.07	-0.55	-0.79	-0.82	0.96	1.26
30	Curve6	2.03	-1.23	5.30	2.37	5.81	-1.27	-1.46	-1.21	1.94	2.28	-0.88	-0.23	-1.03	0.91	1.37	-0.91	-0.45	-1.15	1.02	1.53
31	Curve8	-2.53	-0.47	5.45	2.57	6.03	0.13	-0.62	0.88	0.63	1.08	1.15	-0.56	0.69	1.28	1.45	1.33	-0.67	0.88	1.49	1.73

32	R1	-0.85	-2.34	4.11	2.49	4.81	-0.04	-1.29	-1.11	1.29	1.70	-0.15	-0.69	-1.03	0.71	1.25	-0.38	-0.91	-1.19	0.99	1.55
33	R3	-2.39	2.87	4.57	3.73	5.90	-1.43	0.89	-1.55	1.68	2.29	-1.01	0.44	-0.83	1.10	1.38	-1.20	0.69	-1.11	1.38	1.77
34	R5	-2.59	2.14	3.06	3.36	4.54	-1.45	0.25	-1.93	1.47	2.43	-1.04	0.63	-1.14	1.22	1.67	-0.98	0.92	-1.56	1.34	2.06
35	R7	-3.08	-2.55	2.29	4.00	4.61	-0.77	-0.98	-1.59	1.25	2.02	-0.67	-0.62	-1.25	0.91	1.55	-0.82	-0.33	-1.29	0.88	1.56
36	R9	-2.45	-2.26	5.03	3.33	6.03	-0.99	-0.18	-0.69	1.01	1.22	-0.60	-0.39	-0.58	0.72	0.92	-0.51	-0.55	-1.66	0.75	1.82
37	R11	-2.69	-2.16	2.56	3.45	4.30	-0.73	-0.49	0.66	0.88	1.10	-0.77	-0.58	0.51	0.96	1.09	-0.72	-0.77	0.57	1.05	1.20
38	R13	-3.41	-1.58	-3.30	3.76	5.00	-1.75	-1.24	-1.05	2.14	2.39	-1.35	-0.84	-0.83	1.59	1.79	-0.53	-0.91	-0.93	1.05	1.40
Minimum		-4.20	-4.16	-4.05	0.21	3.34	-1.93	-1.58	-3.03	0.36	0.48	-1.39	-1.43	-1.89	0.66	0.86	-1.73	-1.56	-2.02	0.56	0.63
Maximum		2.41	3.32	6.65	4.95	7.66	2.03	1.59	1.22	2.42	3.05	1.49	1.49	1.56	1.88	2.53	1.48	1.56	1.73	2.18	2.76
Mean		-0.93	-0.96	4.79	1.34	4.97	-0.23	-0.19	-0.35	0.30	0.46	-0.21	-0.17	-0.24	0.27	0.36	-0.21	-0.25	-0.28	0.32	0.43
RMS		**2.20**	**2.34**	**5.32**	**3.21**	**6.22**	**0.98**	**0.97**	**1.12**	**1.38**	**1.78**	**0.87**	**0.83**	**0.98**	**1.20**	**1.55**	**0.97**	**0.91**	**1.09**	**1.32**	**1.72**

Table 3: The summary of the errors against the 23 checking GCPs from (i) the original point cloud, (ii) the original point cloud after the boresight compensation, (iii) refined single strip solution through the feature enhanced 3DCCT after the boresight compensation, and (iv) refined two strips solution through the MA after the boresight compensation (the east segment, 570m, Area 2)

No.	ID	Case 1: Original Differences [cm]					Case 2: Original Differences (after BA) [cm]					Case 3: Single strip refined (after BA) [cm]					Case 4: two-strip refined (after BA) [cm]				
		N	**E**	**U**	**2DH**	**3D**	**N**	**E**	**U**	**2DH**	**3D**	**N**	**E**	**U**	**2DH**	**3D**	**N**	**E**	**U**	**2DH**	**3D**
1	L41	-2.59	-3.27	3.21	4.17	5.26	-2.44	-2.98	2.73	3.85	4.72	-0.88	-0.83	0.73	1.21	1.41	-0.49	-0.74	0.98	0.89	1.32
2	L45	-3.35	-1.95	4.12	3.88	5.66	-2.59	1.47	1.69	2.98	3.42	0.36	0.59	0.92	0.69	1.15	-0.55	0.68	0.88	0.87	1.24
3	L46	-3.11	-2.13	4.40	3.77	5.79	-3.38	-2.08	2.07	3.97	4.48	-0.78	0.47	1.22	0.91	1.52	-0.67	0.69	1.01	0.96	1.39
4	L49	-3.42	-3.16	3.35	4.66	5.74	-2.95	-1.99	0.82	3.56	3.65	-0.37	-0.33	0.82	0.50	0.96	-0.39	-0.88	0.75	0.96	1.22
5	L50	-2.20	-2.95	4.49	3.68	5.81	2.88	-1.95	2.41	3.48	4.23	-1.05	0.44	-1.26	1.14	1.70	-0.98	0.67	-0.93	1.19	1.51
6	R10	-2.03	-2.24	4.81	3.02	5.68	-1.99	2.12	2.19	2.91	3.64	-0.93	0.45	1.35	1.03	1.70	-0.73	0.73	1.23	1.03	1.61
7	R12	-1.91	2.89	4.25	3.46	5.48	-0.89	1.85	2.14	2.05	2.97	-1.02	-1.41	0.47	1.74	1.80	-0.83	-0.48	0.69	0.96	1.18
8	R14	-2.25	-3.62	3.59	4.26	5.57	0.94	-0.88	-1.61	1.29	2.06	0.38	-0.98	0.52	1.05	1.17	0.84	-0.67	0.98	1.07	1.45
9	R16	-3.29	-2.77	-3.16	4.30	5.34	0.78	-1.93	-0.75	2.08	2.21	-0.73	-1.06	-0.89	1.29	1.56	-0.62	-0.71	-1.22	0.94	1.54
10	R17	-1.14	-3.61	-3.48	3.79	5.14	-1.04	-0.64	1.48	1.22	1.92	1.04	-0.62	-0.73	1.21	1.41	0.87	-0.89	-0.51	1.24	1.35
11	R19	3.24	-2.40	3.90	4.03	5.61	1.47	-1.78	2.05	2.31	3.09	0.57	-0.98	-0.88	1.13	1.44	0.69	-1.04	-0.98	1.25	1.59
12	R21	-1.32	-2.62	4.55	2.93	5.41	-1.09	-0.82	2.69	1.36	3.02	-0.66	0.58	0.66	0.88	1.10	-0.41	0.69	0.42	0.80	0.91
13	R22	-1.60	-2.89	4.74	3.30	5.78	-0.31	1.25	2.64	1.29	2.94	-0.97	0.73	1.17	1.21	1.69	-0.57	0.62	1.02	0.84	1.32
14	R25	-3.75	2.41	2.16	4.46	4.95	-1.53	2.47	2.38	2.91	3.76	-1.05	1.11	0.48	1.53	1.60	-0.79	0.78	0.88	1.11	1.42
15	R26	-3.83	2.68	4.99	4.67	6.84	0.91	0.92	2.65	1.29	2.95	-0.53	0.57	1.03	0.78	1.29	-0.64	0.88	1.29	1.09	1.69
16	R29	-3.40	-3.74	2.64	5.05	5.70	-0.62	-1.51	-2.01	1.63	2.59	-0.92	-1.34	-0.67	1.63	1.76	-0.59	-0.92	-1.33	1.09	1.72

17	R30	2.01	-3.04	4.69	3.64	5.94	0.56	-1.38	0.88	1.49	1.73	0.67	0.48	1.05	0.82	1.33	0.58	0.33	0.64	0.67	0.92
18	R200	-1.01	-3.29	5.73	3.44	6.68	-1.14	-1.22	-1.15	1.67	2.03	-0.68	-0.66	-1.17	0.95	1.51	-0.49	-0.57	-1.01	0.75	1.26
19	R203	2.83	-2.35	3.29	3.68	4.94	2.09	-1.77	-2.38	2.74	3.63	0.89	-0.88	-0.63	1.25	1.40	0.83	-0.78	-0.57	1.14	1.27
20	R204	-1.05	-1.98	4.33	2.24	4.88	-0.61	-1.08	1.65	1.24	2.06	-0.28	0.68	-0.48	0.74	0.88	-0.57	0.41	-1.38	0.70	1.55
21	R205	2.31	-1.75	5.14	2.90	5.90	1.71	-1.33	2.99	2.17	3.69	1.09	-0.35	0.82	1.14	1.41	1.03	-0.31	0.77	1.08	1.32
22	R208	-1.90	-2.20	4.87	2.91	5.67	-0.75	-0.63	1.91	0.98	2.15	-0.64	-0.78	0.93	1.01	1.37	-0.51	-0.77	0.87	0.92	1.27
23	R210	-3.76	-3.18	5.32	4.92	7.25	1.45	-0.52	-1.89	1.54	2.44	0.71	-0.44	-1.16	0.84	1.43	0.77	-0.59	-1.09	0.97	1.46
Minimum		-3.83	-3.74	-3.48	2.24	4.88	-3.38	-2.98	-2.38	0.98	1.73	-1.05	-1.41	-1.26	0.50	0.88	-0.98	-1.04	-1.38	0.67	0.91
Maximum		3.24	2.89	5.73	5.05	7.25	2.88	2.47	2.99	3.97	4.72	1.09	1.11	1.35	1.74	1.80	1.03	0.88	1.29	1.25	1.72
	Mean	-1.59	-2.05	3.56	2.59	4.41	-0.37	-0.63	1.11	0.73	1.33	-0.25	-0.20	0.19	0.32	0.37	-0.18	-0.12	0.15	0.22	0.27
	RMS	**2.67**	**2.82**	**4.24**	**3.88**	**5.75**	**1.74**	**1.65**	**2.08**	**2.40**	**3.17**	**0.84**	**0.84**	**0.96**	**1.19**	**1.53**	**0.75**	**0.77**	**1.01**	**1.08**	**1.48**

Hofmann, S. and Brenner, C. (2009): Quality Assessment of Automatically Generated Feature Maps for Future Driver Assistance Systems. 17th ACM SIGSPATIAL International Conference on Advances in Geographic Information Systems, Seattle, Washington, USA, pp. 500–503.

Hu, Baoxin; Jianguo Wang and Guannan Liu (2012): Performance and Potentials of Ground LiDAR (mobile and static) in Engineering Survey and Highway Design, HIIFP, Series Number: HIIFP-113, Ministry of Transportation of Ontario, 2012 (www.library.mto.gov.on.ca).

Hu, Baoxin; Wang, Jianguo; Leslar, Michael and Liu, Guannan (2013): Improving the Accuracy of Mobile LiDAR for Engineering Surveys, LiDAR Magazine, Vol. 3, No. 6.

International Hydrographic Organization (IHO) (2011): Chapter 3 Depth Determination, Manual on Hydrography Publication C-13, 1st ed., IHO International Hydrographic Bureau, Monaco, 2011.

Jaakkola, A.; Hyyppä, J.; Kukko, A.; Yu, X.; Kaartinen, H.; Lehtomäki, M. and Lin, Y. (2010): A Low-Cost Multi-Sensoral Mobile Mapping System and Its Feasibility for Tree Measurements, ISPRS Journal of Photogrammetry and Remote Sensing, Vol.65, pp. 514–522.

Kadatskiy, A. Flower (2011): Accuracy and Error Assessment of Terrestrial, Mobile and Airborne LiDAR, ASPRS 2011 Annual Conference, Milwaukee, May 2011.

Kager, H. (2004): Discrepancies between Overlapping Laser Scanning Strips Simultaneous Fitting of Aerial Laser Scanner Strips, Proceedings of the International Society for Photogrammetry and Remote Sensing XXth Congress, Istanbul, 34(B/1): 555 - 560.

Kenza, Ait EL Kadi and Quaziz Mohamed (2018): The estimation of theoretical accuracy of mobile terrestrial LiDAR, African Journal of Land Policy and Geospatial Sciences, Issue 1, pp. 51-65, 2018.

Keller, F. and Sternberg, H. (2013): Multi-Sensor Platform for Indoor Mobile Mapping: System Calibration and Using a Total Station for Indoor Applications, Remote Sensing, Volume 5, p. 5805-5824, 2013.

Kersting, A. P.; Zhai, R. and Habib, A. (2008): Strip Adjustment Using Conjugate Planar and Linear Features in Overlapping Strips, ASPRS 2008 Annual Conference, Portland, Oregon, 2008.

Khanal., M., Hasan, M., Sterbentz, N., Johnson, R., & Weatherly, J. (2020): Accuracy comparison of aerial LiDAR, mobile-terrestrial LiDAR, and UAV photogrammetric capture data elevations over different terrain types, *Infrastructures*, *5*(8), 65.

Kilian, J.; Haala, N. and Englich, M. (1996): Capture and Evaluation of Airborne Laser Scanner Data. International Archives of Photogrammetry and Remote Sensing, Vol. XXXI, B3, 383 – 388, Vienna, Austria.

Kornus, W. and Ruiz, A. (2003): Strip Adjustment of LiDAR Data, International Archives of Photogrammetry and Remote Sensing, Working Group III/3 Workshop, Dresden, Germany, International Society of Photogrammetry and Remote Sensing (ISPRS).

Kucak, Ramazan; Serdar Erol and Bihter Erol (2022): The Strip Adjustment of Mobile LiDAR Point clouds using iterative closest point (ICP) algorithm, Arabian Journal of Geosciences, 15, 1017(2022).

Kurdi, Fayez T.; Paul Reed; Zahra Gharineiat and Mohammad Awrangjeb (2023): Efficiency of Terrestrial Laser Scanning in Survey Works: Assessment, Modelling, and Monitoring, International Journal of Environment Sceinces & Natuaral Resources, Vol. 32, Issue 2, 2023.

Lee, Jaebin; Yu, Kiyun; Kim, Yongil and Habib, Ayman F. (2007): Adjustment of Discrepancies between LiDAR Data Strips Using Linear Features. IEEE Geoscience and Remote Sensing Letters, Vol. 4, No. 3, 475 – 479, 2007.

Leslar, Michael; Wang, Jianguo; and Hu, Baoxin (2011): *Comprehensive Utilization of Temporal and spatial domain Outlier Detection Methods for Mobile Terrestrial LiDAR Data*, Remote Sensing, 2011, 3, pp. 1724-1742.

Leslar, Michael; Baoxin Hu and Jianguo Wang (2014): Error Analysis of a Mobile Terrestrial LiDAR System, Geomatica, 68(3):183-194, 2014.

Leslar, Michael; Jianguo Wang and Baoxin Hu (2016): Boresight and Lever Arm Calibration of a Mobile Terrestrial LiDAR System, Geomatica, 70(2): 97-112, 2016.

Leslar, Michael (2016): Improvement of the Geospatial Accuracy of Mobile Terrestrial LiDAR Data, PhD Dissertation, York University, 2016.

Liu, Guannan (2015): Accuracy Improvement of Terrestrial Mobile LiDAR System in Engineering Surveys, MSc. Thesis, York University, 2015.

MTO (2016): Engineering Survey Manual., Geomatics Office, Highway Standards Branch, Provincial Highways Management Division, Ministry of Transportation of Ontario (MTO), St. Catharines, Ontario, 2016.

OpTech (2012): Summary Specification Sheet of Lynx Mobile Mapper, OpTech Inc, 2012.

Pfeifer, N., S. O. Elberink, and S. Filin (2005): Automatic Tie Elements Detection for Laser Scanner Strip Adjustment. International Archives of Photogrammetry and Remote Sensing, 36(3/W3): 1682-1750.

Pothou, A., C. Toth, S. Karamitsos and A. Georgopoulos (2009): Spatial Distribution Requirements of Reference Ground Control for Estimating LiDAR/INS Boresight Misalignment. Special Issue on Mobile Mapping Technology, Vol. 15, No. 5, pp. 776 – 789.

Reshetyuk, Yuriy (2006): Investigation and Calibration of Pulsed Time-of-flight Terrestrial Laser Scanners, Royal Institute of Technology (KTH), Department of Transport and Economics, Division of Geodesy.

Rybka, Y (2011): Autodesk and Bentley Systems Talk about Mobile LiDAR, LiDAR, 1(2), 41-44.

Shan J. and Toth, C.K. (2008): Topographic Laser Ranging and Scanning, CRC Press, 2008.

Sherif, E., A. Moussa, D.D. Lichti and N. El-Sheimy (2011): Detection of Road Curb from Mobile Terrestrial Laser Scanner Point Cloud. International Archives of the Photogrammetry, Remote Sensing and Spatial Information Sciences, Vol. XXXVIII-5/W12, Workshop, 29-31 August, Calgary, Canada.

Slob, S. and R. Hack (2004): 3D Terrestrial Laser Scanning as a New Field Measurement and Monitoring Technique, Engineering Geology for Infrastructure Planning in Europe: A European Perspective, Edited by Robert Hack, Rafig Azzam, and Robert Charlier. Lecture Notes in Earth Sciences, Vol. 104, pp.179-189.

Teo, Tee-Ann; Hsien-Ming Wu (2018): Radiometric Block Adjustment for Multi-Strip Airborne Waveform Lidar Data, Remote Sensing, 2015, 7, 16831-16848.

Vosselman, G. (2002): Strip Offset Estimation Using Linear Features, 3rd Intl Workshop on Mapping Geo-Surfical Processing using *Laser Altimetry*, 2002.

Wang, Jianguo; Weining Qiu; Yibin Yao and Yun Wu (2019): Error Theory and Foundation of Surveying Adjustment, Textbook, Wuhan University Press, 2019.

Yousif, H.; J. Li; M. Chapman and Y. Shu (2010): Accuracy Enhancement of Terrestrial Mobile LiDAR Data Using Theory of Assimilatrion, International Archives of Photogrammetry, Remote Sensing and Spatial Information Sciences, Vol. XXXVIII, Part 5 Commission V Symposium, Newcastle upon Tyne, UK. 2010.

Authors

Jianguo Wang is a Professor in Geomatics Science and Engineering at the Department of Earth and Space Science and Engineering, York University, Canada. He holds a Dr.-Ing. in Surveying Engineering from the Universität der Bundeswehr München, Germany, a B.Eng. and a M.

Eng. in Surveying Engineering from WTUSM (Wuhan Technical University of Surveying and Mapping. His current research interests include multisensor integrated kinematic positioning and navigation, optimal estimation methods, and data fusion, and statistical learning,

Guanan Liu currently works as a Project Surveyor at Geomatics Central department, Ministry of Transportation Ontario. She is a licensed Ontario Land Surveyor (OLS), and holds a MSc and Bachelor's Degree in Geomatics Engineering from York University, Canada.

Baoxin Hu is a Professor in Geomatics Science and Engineering at the Department of Earth and Space Science and Engineering, York University, Canada. She holds a Ph.D. in Remote Sensing from Boston University, USA, and a MEng. and a BEng. in Electrical Engineering from Tianjin University, China. Her research interests include segmentation and classification using multi-source remotely sensed data, information fusion, 3D scene reconstruction, and deep learning.